Desalination and Water Treatment
www.deswater.com
doi: 10.1080/19443994.2013.769705

51 (2013) 6837–6845
October

Taylor & Francis
Taylor & Francis Group

Thermal properties and phosphate adsorption efficiency of coarse aluminum silicate fraction

Tiina Leiviskä[a,*], Arja Sarpola[a], Eetu Heikkinen[b], Juha Tanskanen[a]

[a]*Chemical Process Engineering Laboratory, Department of Process and Environmental Engineering, University of Oulu, P.O. Box 4300, FI-90014, Oulu, Finland*
Tel. +358 0294482386; Fax: +358 85532304; email: tiina.leiviska@oulu.fi
[b]*Laboratory of Process Metallurgy, Department of Process and Environmental Engineering, University of Oulu, P.O. Box 4300, FI-90014, Oulu, Finland*

Received 8 February 2012; Accepted 14 January 2013

ABSTRACT

A clay deposit from Poskimäki (PM, Puolanka, Finland) was fractionated, and the coarse fraction (size 0.02–2 mm) was characterized to find potential applications in water or waste water treatment. The coarse fraction contained mainly quartz, kaolinite, and iron-containing compounds. Thermal behavior was investigated by simultaneous thermogravimetric analysis and differential scanning calorimetry (TGA–DSC). The observations were supported by thermodynamic calculations executed with FactSage and HSC software and their databases. TGA–DSC analyses verified the differences between the untreated and annealed (800°C) samples. Kaolinite transformed into amorphous metakaolinite at 450–600°C. Phase transformations also occurred at a lower temperature range (240–320°C) with the PM sample. TGA–DSC data suggested the use of different annealing temperatures for the modification of the PM sample. The PM samples (non-annealed, 185, 360, 800°C) were tested as adsorbents for the removal of phosphate from water. The PM-a360 sample had the highest specific surface area and worked best in phosphate removal. The phosphate adsorption efficiency increased with decreasing pH.

Keywords: Iron oxide minerals; Thermal properties; Adsorption; Phosphate

1. Introduction

Phosphorus is a nutrient essential for plant growth and in excess causes eutrophication of water bodies. Phosphorus is often found in natural aquatic environments mainly as orthophosphates, including organic phosphate and polyphosphate. Conventional technologies for the removal of phosphorus include coagulation–flocculation, e.g. with iron and aluminum chemicals, and biological phosphorus removal. Adsorption and ion exchange are also well-known technologies in water and waste water treatment for different types of pollutants. The general trend worldwide is to develop cheap adsorbents and ion exchange resins from locally available materials such as agricultural wastes, clay materials, and industrial waste products to increase the cost efficiency of treatment. Several adsorbents have been tested for the removal of phosphorus from aqueous solution, such as aluminum oxides [1], iron oxides [1–6], spent alum sludge [7], La(III)-loaded granular ceramic adsorbent [8],

*Corresponding author.

zirconium hydroxide [9], and MgMn-layered double hydroxide [10].

Phosphate adsorption on iron (III) hydroxide minerals has been widely investigated, because these materials control phosphorus mobility in nature as well as being utilized in water and waste water treatment processes. Zeng et al. [11] reported that iron oxide tailings removed phosphate efficiently from aqueous solutions and the desorbability of phosphate from the material was low. Boujelben et al. [2] showed that iron oxide-coated sand (synthetic and natural) and iron oxide-coated crushed brick could be used as a low-cost adsorbent for phosphate removal. The proposed mechanism for phosphate adsorption on the surfaces of the iron oxyhydroxide is that the phosphate ion binds to two Fe^{3+} ions via two oxygen ions and two hydroxyl groups are replaced [3,4]. In addition, electrostatic interaction with a charged surface has been considered in the literature [11,5]. Increased crystallinity of iron particles has been reported to have an adverse effect on phosphate adsorption [1].

Previously we studied the remaining coarse fractions (size 0.02–2 mm) of the kaolin enrichment process and discussed their potential applications in water and waste water treatment as low-cost adsorbents [12]. The deposits were collected from two places in Puolanka, located in the Kainuu region of Finland: Pihlajavaara (PV) and Poskimäki (PM). The coarse fractions contained mainly quartz and the kaolinite content was quite low. The PM sample had a higher specific surface area (SSA) and cation exchange capacities than the PV sample due to a higher amount of iron. It was concluded that the coarse PM sample could be utilized in water treatment, for example as a raw material in iron oxide-coated sands. Using these leftovers to produce water treatment chemicals could lead to savings in resources and cost reduction. Any possible chemical or physical modification should be kept as simple as possible to avoid additional costs.

The first objective of this study was to characterize the wet fractionated PM sample by investigating its thermal behaviour by simultaneous thermogravimetric analysis and differential scanning calorimetry (TGA–DSC). The TGA–DSC data suggested the use of different annealing temperatures for the PM sample modification. The effect of annealing on the mineralogy and surface area was studied. The second objective of this study was to assess the feasibility of using PM samples (non-annealed, 185, 360 and 800˚C) for the removal of phosphate from synthetic aqueous solutions. In addition, the linear and nonlinear method of Langmuir and Freundlich isotherms were used for data fitting.

2. Experimental

2.1. Pre-treatment and characteristics of clay samples

The kaolin sample was collected from Puolanka, Poskimäki (PM) 64˚ 38´, located in the Kainuu region of Finland. The pre-treatment of the sample was performed by wet fractionation. In the wet fractionation method, the sample was first passed through a 2-cm sieve and then through a 2-mm sieve. The <2 mm fraction was wet fractionated by sedimentation. About 20 kg of clay sample was added to 100 L of water and mixed for 3 h at 60 rpm. Then the suspension was allowed to settle for 12 min and 12 s before separating the settled sediment and the solution. The kaolinite group minerals were enriched in the fine fractions and remaining coarse fraction (20 μm–2 mm, in the sediment) was used in this research. The coarse fraction was dried for 48 h at 150˚C. After that the sample was ball milled with steel grinding balls (50 mm in diameter).

The wet-fractionated coarse PM sample was light brown. The PM sample had a multimodal particle size distribution; the maxima were 88, 35, 12, and 2 μm [12]. Half of the sample was annealed (referred to as "a" when considering samples) at 800˚C for 4 h in the presence of air. After TGA–DSC analyses, PM was also annealed at 185˚C (PM-a185) and 360˚C (PM-a360) for 4 h in an air atmosphere.

2.2. TGA–DSC analyses

TGA–DSC equipment (Netzsch STA 409 PC Luxx) with a quadrupole mass spectrometer (Netzsch QMS 203 C Aëolos) was used for thermogravimetric measurements of the change in weight of the sample as a function of temperature as well as to observe thermal events (endothermic or exothermic) such as changes in crystal structures. All the tests were executed in an air atmosphere with a flow rate of 60 mL/min. Samples of approximately 30 mg were placed in Pt crucibles and the temperature was increased at a rate of 20˚C/min from 30˚C to 1,200˚C. The gases that evaporated from the samples during heating were measured with the mass spectrometer. The key fragment ions that were considered are presented in Table 1. Commercial metakaolinite, Metamax (BASF), was used as a reference material in the TGA–DSC analyses.

2.3. Thermodynamic calculations

To support the TGA–DSC analyses, the most thermodynamically stable phases of the Fe–Si–Al–O–H-system were defined in a temperature range of 200˚C

Table 1
The key fragment ions measured in TGA–DSC analyses

Ion	Mass/charge-ratio (m/e)	Indication of …
C^+	12	… carbonate decomposition
OH^+	17	… moisture or crystal water removal or hydroxide decomposition
H_2O^+	18	… moisture or crystal water removal or hydroxide decomposition
Ar^+	40	Used as an internal standard
CO_2^+	44	… carbonate decomposition

to 1,200°C using the computational thermodynamic software FactSage Version 5.5 and its databases. The software, its database and its possibilities and restrictions are presented thoroughly elsewhere by the authors of the software [13]. Initial compositions for the calculation were chosen according to the X-ray fluorescence (XRF) analyses of the sample. The only possible phases considered in all the calculations were a gas phase that was assumed to behave ideally and all the pure solid and liquid compounds of the Fe–Si–Al–O–H system included in the FactSage databases. The pressure was considered constant at 101.3 kPa (1 atm). The proportional amounts of the elements were chosen according to the samples used in the experiments.

2.4. Adsorption studies

In the adsorption experiments, the coarse PM fractions were dispersed in 200 mL of phosphate solution. KH_2PO_4 (Merck) was used as the source of phosphate. The solution pH was set up beforehand with HCl or NaOH. The dispersions were shaken 24 h at room temperature (22°C). The dispersions were then centrifuged for 10 min at 500 *g* and a sample was taken from the top for analysis (pH_{24h} and phosphate phosphorus (PO_4–P)). Each experiment was performed in duplicate and the average is presented in the figures, with the error bar representing the standard deviation (except Fig. 5).

Isotherm studies were conducted with varying phosphate concentrations with an adsorbent dosage of 2 g/L at an initial pH of 4.8. The effect of the adsorbent was studied by varying the dosage from 2 to 10 g/L at an initial pH of 4.8 (10 mg/L PO_4–P). The effect of the initial pH (2.8–4.8) on PO_4–P uptake (10 mg/L solution) was studied at a constant dosage (6 g/L). Commercial Kemira CFH-12 was used as a reference material in the adsorption studies. CFH-12 consists of FeOOH granules of 1–2 mm in size and an iron content of approximately 48%.

2.5. Adsorption modeling

The linear least-squares method and a non-linear method of two commonly used isotherms, Langmuir and Freundlich, were investigated in this research. The Langmuir isotherm is expressed by the following equation (Eq. (1)):

$$q_e = \frac{q_m b C_e}{1 + b C_e} \tag{1}$$

where q_e is the equilibrium adsorption capacity (mg/g); C_e is the aqueous phase concentration (mg/L); q_m is the maximum adsorption capacity (mg/g); b is the adsorption equilibrium constant (L/mg). The Langmuir isotherm equation can be linearized into four forms [14], but only one very common form (Langmuir 1) was used in this study (Eq. (2))

$$\frac{C_e}{q_e} = \frac{C_e}{q_m} + \frac{1}{q_m b} \tag{2}$$

The Freundlich isotherm and its linear form can be written as (Eqs. (3) and (4)):

$$q_e = K_F C_e^{1/n} \tag{3}$$

$$\log(q_e) = \log(K_F) + 1/n \log(C_e) \tag{4}$$

where C_e is the equilibrium concentration in the solution (mg/L); q_e is the equilibrium adsorption capacity (mg/g); K_F ((mg/g)(L/mg)$^{1/n}$) and $1/n$ are empirical constants.

The Gibbs free energy change is obtained by the following equation (Eq. (5)):

$$\Delta G^\circ = -RT \ln b \tag{5}$$

where R is the gas constant (8.314 J/mol K); T is the temperature (in this study 295.15 K), and b is the equilibrium constant obtained from the Langmuir equation. The negative ΔG° value means the sorption process is spontaneous.

The non-linear regression was performed using the Microsoft Excel Solver tool. In practice, the residual sum of squares was minimized by adjusting the model parameters. Chi-square analysis was performed to compare the experimental data with model predictions in accordance with Ho [14] (Eq. (6)):

$$\chi^2 = \Sigma \frac{(q_e - q_{e,m})^2}{q_e} \quad (6)$$

where q_e is the equilibrium capacity (mg/g) from the experimental data and $q_{e,m}$ the equilibrium capacity obtained with a model (mg/g). If the calculated values from the model are similar to the experimental data, the chi-square is small.

2.6. Other measurements

The X-ray diffraction (XRD) measurements were performed using a Siemens D5000 diffractometer (Siemens, Karlsruhe, Germany) equipped with a copper target X-ray tube, using a 40 kV voltage, and 40 mA current. The samples were measured at room temperature in the 2θ range from 2° to 60° with a step size of 0.010 and a step time of 1 s. The phases were identified using the DIFFRAC plus EVA software and an ICDD data file (rev. 2006).

In the XRF analyses, 7.5 g of powdered samples were mixed with beeswax and pressed into pellets using 10 metric tons of power. The sample pellets were analyzed on a Bruker AXS Pioneer S4 XRF spectrometer (Karlsruhe, Germany) using the Spectra plus software.

The SSA of the PM samples was measured by the BET nitrogen adsorption technique at −195.8°C with an ASAP 2020 surface area and porosity analyser (Micromeritics). The phosphate phosphorus was measured using the ammonium molybdate spectrometric method with an Aquakem 600 analyser (Thermo Scientific). The detection limit was 2 μg/L.

3. Results and discussion

3.1. Characteristics of PM samples

Table 2 shows the chemical composition of the PM samples studied according to the XRF analyses. The FeO content was 10.2–10.6% (about 8% iron) in all samples and the Al_2O_2 content was 15.7–16.2%. The SiO_2 content was slightly higher in the PM-a800 (66.7%) than in the others (60.7–63.1%).

Table 3 shows the effect of annealing on SSA and mineral composition. According to XRD [12], PM included mainly quartz, some kaolinite, illite, anorthite, and nacrite. The amount of amorphous material was low according to XRD and thus the majority of the iron was probably attached to the minerals by replacing another element. The SSA of PM was 22.1 m^2/g. The PM-a185 and PM-a360 included mainly quartz and some kaolinite, illite and clinochlore. The SSA first decreased at 185°C and then increased at 360°C. The PM sample annealed at 800°C had a lower SSA, and the Fe compounds transformed to hematite according to XRD [12].

Table 2
Chemical compositions of PM samples according to the XRF

Sample	PM	PM-a185	PM-a360	PM-a800
Na_2O (%)	0.09	0.09	0.08	0.11
MgO (%)	2.22	2.25	2.19	2.18
Al_2O_3 (%)	15.85	16.23	16.03	15.69
SiO_2 (%)	61.00	60.72	63.13	66.69
P_2O_5 (%)	0.18	0.19	0.18	0.19
K_2O (%)	1.61	1.57	1.57	1.61
CaO (%)	0.14	0.15	0.15	0.15
TiO_2 (%)	0.45	0.44	0.45	0.47
Cr_2O_3 (ppm)	99	99	111	111
MnO (%)	0.11	0.11	0.10	0.11
FeO (%)	10.23	10.21	10.31	10.67
Ba (ppm)	594	569	573	603
Sum	91.94	92.01	94.26	97.93

Table 3
The effect of temperature on surface area and mineral composition

Sample	SSA (m^2/g)	XRD
PM	22.1	Quartz, Kaolinite, Illite, Anorthite Na-rich, Nacrite
PM-a185	19.0	Quartz, Kaolinite, Illite, Clinochlore
PM-a360	28.9	Quartz, Kaolinite, Illite, Clinochlore
PM-a800	16.2	Quartz, Illite, Hematite

3.2. Thermal behaviour

Thermal treatment is one option for improving the properties of adsorbents. Thermal behaviour was studied by TGA–DSC for the PM sample (Fig. 1) and its annealed (800°C) form (Fig. 2). The non-annealed PM sample had two weight loss areas. The first main weight loss of the PM sample occurred at a range of 240–320°C and the second one at a range of 450–600°C. The weight losses corresponded well with the peak of the OH^+ curve in the mass spectrometric analyses. This indicated that the weight loss of the sample is a consequence of the water that was removed from the sample.

Between 450°C and 600°C, the weight loss was probably due to the dehydroxylation of kaolinite into

amorphous metakaolinite. This reaction also showed up on DSC at approximately 520˚C as an endothermic event (Fig. 1), which is in agreement with the results reported previously [15]. The corresponding weight loss and the endothermic peak were not observed with the annealed sample (Fig. 2) and Metamax (data not shown) due to the irreversible nature of the reaction. Also the XRD analyses verified the disappearance of kaolinite in the PM-a800 sample [12].

Previously, on the grounds of XRD, we could not state with certainty whether these coarse samples contained kaolinite or dickite or both of them. Dickite belongs to the kaolinite group and has the same composition as kaolinite but a different crystal structure. The dehydroxylation temperature of dickite to metadickite is higher, 700˚C, according to Shoval et al. [16]. Thus, the lower dehydroxylation temperature observed in this study refers to kaolinite and not to dickite.

The exothermic peak at approximately 1,000˚C was probably due to the formation of crystalline phases (mullite). This peak was also verified with Metamax as well as with computational stability analyses which also indicated the formation of mullite at the higher temperatures. The presence of the metastable phases was not perceived with the computational investigations since only the most thermodynamically stable phases were considered.

PM and PM-a800 both had an endothermic peak at 580–581˚C. This peak originated probably from the reversible change of α-quartz to β-quartz [17,18]. To verify this, one experiment was conducted with a kaolin sample (different sample however than was studied in this paper) by first heating to 800˚C and then cooling. A hysteresis phenomenon was observed. During the cooling period, an exotherm occurred at a slightly lower temperature than the corresponding endothermic one. The change in the crystal structure of the quartz was also supported by the results of the computational stability investigations.

The weight loss at the lower temperature in PM samples was probably due to changes in iron species. This reaction was endothermic and the peak on the DSC curve was found at 319.9˚C (Fig. 1). At the same temperature as the corresponding weight loss, the OH^+ and CO_2^+ curves had peaks indicating that water and carbon dioxide were removed from the sample.

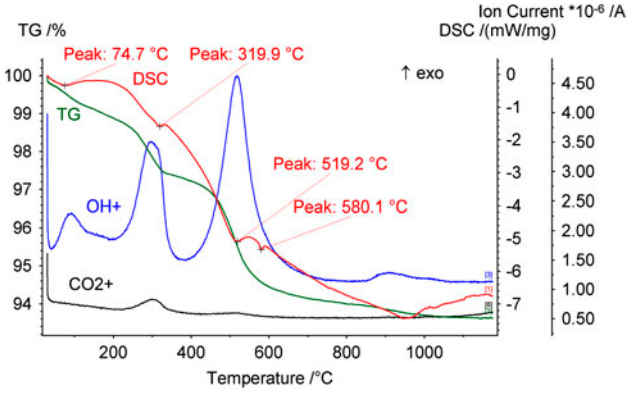

Fig. 1. TGA–DSC curve for PM.

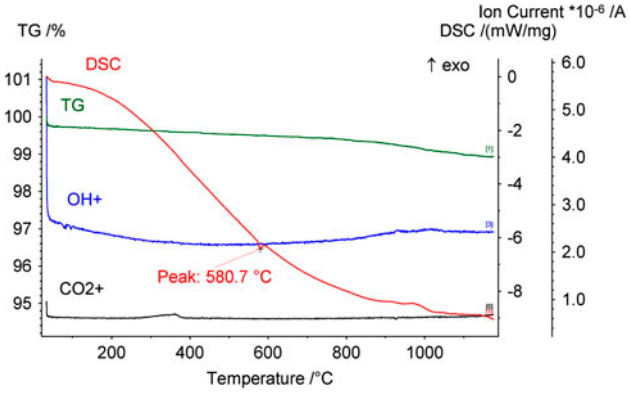

Fig. 2. TGA–DSC curve for PM-a800.

3.3. Adsorption efficiency

The effect of the initial PO_4–P concentration (0–22 mg/L, initial pH 4.8) on the uptake by PM and its annealed forms and CFH-12 with 2 g/L is presented in Fig. 3, which shows that the commercial CFH-12 is considerably more efficient. The CFH-12 had a sixfold amount of iron in comparison with the PM coarse fractions. With 10 mg/L PO_4–P, the

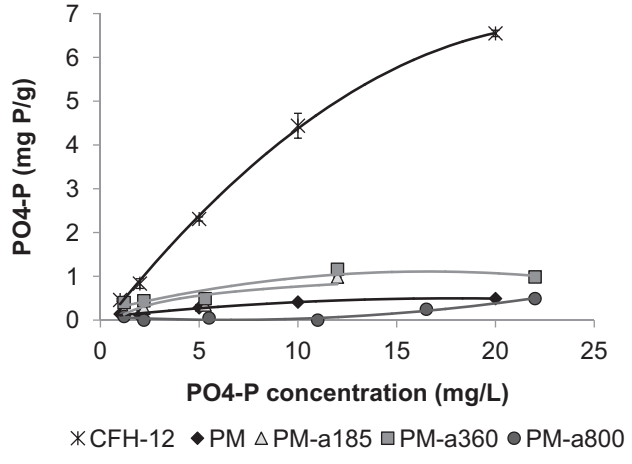

Fig. 3. Adsorption isotherm of PO_4–P with 2 g/L adsorbent (pH_{24h} = 5.2–6.3).

removal efficiency with CFH-12 was about 90%. Of all the PM samples, the PM-a360 worked best. Besides iron oxides, some other components, for example the kaolinite, in the PM samples also contributed to phosphate removal but probably only to a small extent.

Next the adsorbent dosage was compared with to the annealed PM samples (Fig. 4) with a constant 10 mg/L PO_4–P concentration (initial pH 4.8). The adsorption efficiency grew with an increase in adsorbent dosage from a very low level to about 40% reduction, probably due to the increased amount of available adsorbent surface, and again PM-a360 was the most efficient of the PM samples studied.

The effect of pH was also studied with annealed PM samples (6 g/L). The PO_4–P uptake increased as the pH was decreased (Fig. 5). A 56% reduction of PO_4–P was achieved at pH 3.2 with PM-a360 and the maximum adsorption capacity was 0.92 mg P/g.

The pH_{24h} after adsorption was always somewhat higher (0.2–1 units) than the initial pH of 10 mg/L

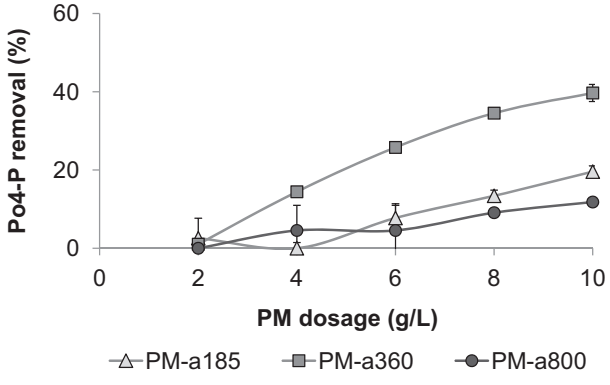

Fig. 4. Effect of adsorbent dosage on 10 mg/L PO_4–P adsorption (pH_{24h} = 5.4–6.3).

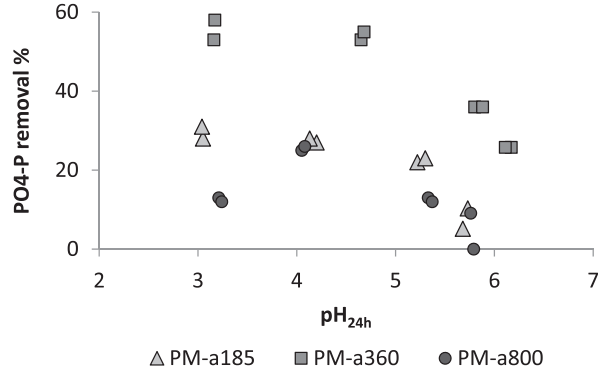

Fig. 5. Effect of pH on PO_4–P adsorption. The adsorbent dosage was 6 g/L and the initial PO_4–P concentration was 10 mg/L. Both repetitions are shown in the figure due to a slight difference in the pH_{24h} values.

PO_4–P solution. The pH_{24h} is presented in Fig. 5. The pH increase referred to the ligand exchange mechanism. The lower efficiency at higher pH might be due to the competition of hydroxide ions with phosphate ions for adsorption sites. If electrostatic mechanism existed, the higher efficiency at lower pH can also be attributed to the fact that with a decrease in the pH, more cationic surface charge sites were available. For some iron species, the reported isoelectric points (IEP) are 5.5–8.9 for hematite (Fe_2O_3), 3.8−6.5 for magnetite (Fe_3O_4), and 6.2–9.6 for goethite (α-FeOOH) [19]. The corresponding point of zero net proton charge values are 8.4 for hematite and 7.7 for goethite [20]. The variation in IEP values (and different zero charge points) in the literature is often due to the different purity level of the samples.

The investigations on PO_4–P adsorption on coarse samples showed the potential usage of PM-a360 in anion adsorption. Even though the material lags behind the commercial product, the results were interesting, because the sample is a leftover from the kaolin clay enrichment process and thus is a cheap material. The material could be used for example to enhance phosphorus removal from peat harvesting runoff or pretreated waste water in a constructed wetland system [21]. The leaching experiments showed that very small amounts of elements (Al, Si, Ca, Mg, K, Cd, Co, Fe, Mn, Cr, Ni, Cu, Zn, Pb, Ba) were dissolved from samples at natural pH values [12]. In the future there is need to study in more detail the iron species after different annealing temperatures. An amorphous iron compounds have been reported to result in greater adsorption capacities than crystalline iron compounds [1,11].

3.4. Adsorption models

The linear Langmuir 1 and Freundlich isotherm constants obtained are presented in Table 4. The fitting data for PM-a185 and PM-a800 is not shown due to its worse adsorption efficiency. In case of the CFH-12 and PM-a360, the Langmuir linear equation yields better fit than the Freundlich linear equation. The Freundlich linear model provided a poor fit for the PM-a360 (r^2 = 0.756). For the PM material both models were fitted to experimental data satisfactorily. Figs. 6–8 show the linear isotherms with the experimental data.

According to the linear Langmuir model, the maximum adsorption capacity (q_m) for the PO_4–P at an initial pH of 4.8 was 6.7 mg/g for CFH-12, 0.8 mg/g for PM-a360 and 0.6 mg/g for PM. The adsorption capacities of the PM materials are at the same level as that reported for Tunisian natural iron oxide-coated sand

Table 4
Isotherm parameters using the linear methods

Isotherm	Material	CFH-12	PM	PM-a360
Langmuir 1 linear	q_m (mg/g)	6.7	0.6	0.8
	b (L/mg)	6.478	0.293	1.285
	r^2	0.996	0.987	0.928
	ΔG° (kJ/mol)	−4.585	3.009	−0.615
	χ^2	1.829	0.022	0.569
Freundlich linear	$1/n$	0.345	0.399	0.272
	K_F ((mg/g)(L/mg)$^{1/n}$)	4.315	0.157	0.456
	r^2	0.920	0.991	0.756
	χ^2	0.766	0.003	0.229

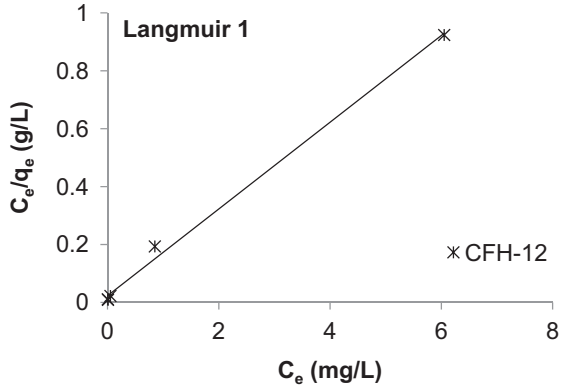

Fig. 6. Linear Langmuir 1 isotherm for the adsorption of phosphate onto CFH-12.

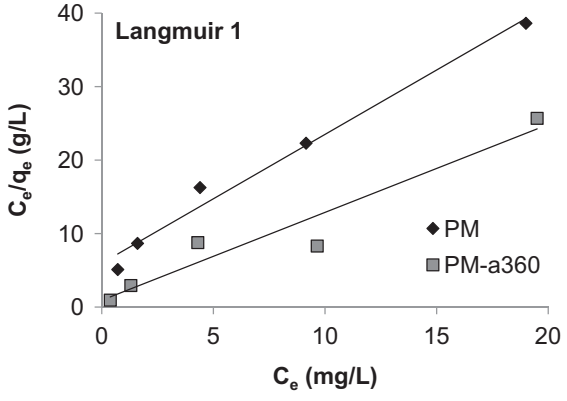

Fig. 7. Linear Langmuir 1 isotherm for the adsorption of phosphate onto PM and PM-a360.

(0.29 mg P/g), synthetic iron oxide coated sand (0.49 mg P/g), and for iron oxide-coated crushed brick (0.59 mg P/g) [2].

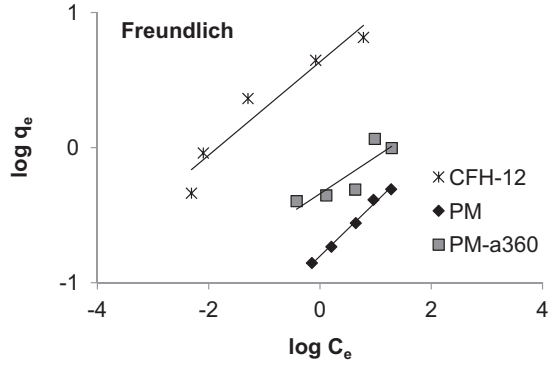

Fig. 8. Linear Freundlich isotherms for the adsorption of phosphate onto CFH-12, PM and PM-a360.

Table 5
Isotherm parameters using the non-linear methods

Isotherm	Material	CFH-12	PM	PM-a360
Langmuir non-linear	q_m (mg/g)	5.884	0.566	1.537
	b (L/mg)	11.582	0.291	0.218
	r^2	0.952	0.980	0.853
	χ^2	0.657	0.023	0.818
Freundlich non-linear	$1/n$	0.262	0.387	0.382
	K_F ((mg/g)(L/mg)$^{1/n}$)	4.214	0.162	0.410
	r^2	0.977	0.992	0.913
	χ^2	0.514	0.003	0.153

CFH-12 and PM-a360 had a negative ΔG° value (Table 4), which means the sorption was spontaneous. The K_F values obtained by the linear Freundlich model showed the same trend as that of q_m for the phosphate adsorption. The values of the n parameter in the Freundlich model indicate whether the sorption is favourable. In the case of good adsorption characteristics, n is between 2 and 10 [22]. The calculated n values lies in that range, denoting good adsorption characteristics of the materials concerned.

Table 5 shows the fitted values of the parameters in the non-linear Langmuir and Freundlich models and the correlation coefficients (r^2). For CFH-12 and PM-a360 the r^2 is higher with linear Langmuir whereas the non-linear Freundlich provided better fit as compared to the linear Freundlich model. For the PM material the non-linear correlation coefficients are at the same level as those of the linearized isotherm model. Figs. 9–11 show the non-linear isotherms with the experimental data.

Tables 4 and 5 also show the chi-square values for each case. The chi-square values of CFH-12 were

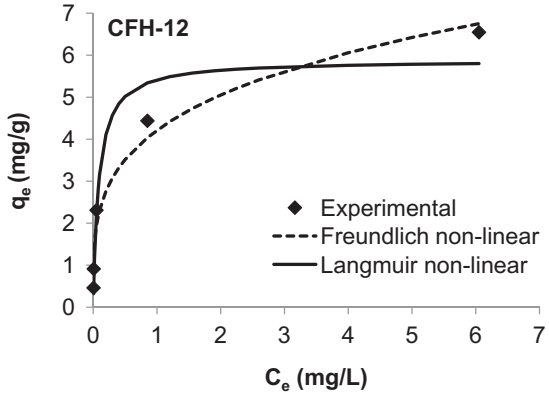

Fig. 9. Non-linear Langmuir and Freundlich isotherms for the adsorption of phosphate onto CFH-12.

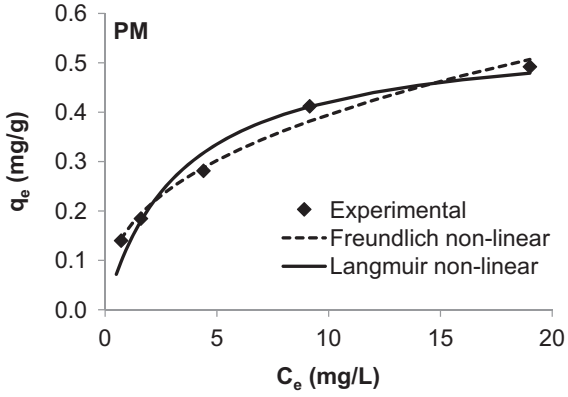

Fig. 10. Non-linear Langmuir and Freundlich isotherms for the adsorption of phosphate onto PM.

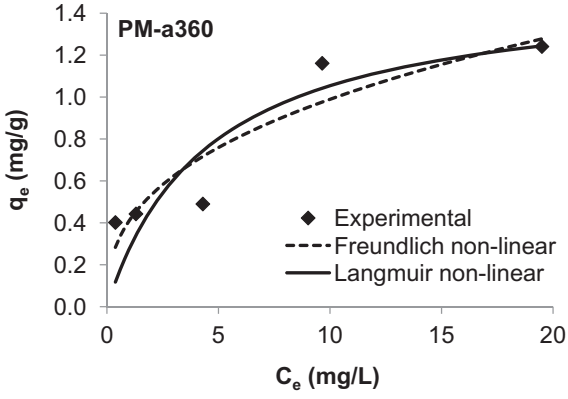

Fig. 11. Non-linear Langmuir and Freundlich isotherms for the adsorption of phosphate onto PM-a360.

lower with non-linear models. The chi-square values of PM were very low and at the same level for linear and non-linear models. For PM-a360 the chi-square value was lower with linear Langmuir than non-linear Langmuir. With the Freundlich model there was the opposite trend.

To summarize the adsorption modeling results, the linearized Langmuir 1 isotherm and non-linear Freundlich isotherm were the most suitable models for characterizing the adsorption of phosphate on CFH-12 and PM-a360. For the PM material, all the studied equations were fitted to experimental data satisfactorily.

4. Conclusions

In this investigation, the aim was to evaluate the adsorption properties and thermal behavior of coarse fraction, which was leftover from kaolin enrichment process. By means of TGA–DSC data, two extra annealing temperatures were chosen for the PM sample. The PM annealed at 360˚C had the highest SSA and higher capacity for phosphate than the other samples (non-annealed, 185˚C, and 800˚C). Even though the coarse PM sample and its annealed forms had rather low capacities for phosphate as compared to commercial FeOOH granules, the material is inexpensive and the modification method for phosphate adsorption is simple. The high temperature used in modification requires, however, a substantial amount of energy and therefore a detailed life cycle cost analysis should be performed next for this method. In addition the optimization of the annealing temperature and the dominant iron species at each temperature should be studied in more depth in the future.

Acknowledgments

The authors would like to thank the Provincial Government of Oulu, the Council of the Oulu Region, the City of Oulu, the European Regional Development Fund, and the Academy of Finland for funding this research and Tuomo Pikkarainen from Morenia Ltd. for his inspiring discussions.

References

[1] M. Arias, J. Da Silva-Carballal, L. García-Río, J. Mejuto, A. Núñez, Retention of phosphorus by iron and aluminum-oxides-coated quartz particles, J. Colloid Interface Sci. 295 (2006) 65–70.
[2] N. Boujelben, J. Bouzid, Z. Elouear, M. Feki, F. Jamoussi, A. Montiel, Phosphorus removal from aqueous solution using iron coated natural and engineered sorbents, J. Hazard. Mater. 151 (2008) 103–110.
[3] R.L. Parfitt, R.J. Atkinson, R. St.C. Smart, The mechanism of phosphate fixation by iron oxides, Soil Sci. Soc. Am. J. 39 (1975) 837–841.
[4] J. Kim, W. Li, B.L. Philips, C.P. Grey, Phosphate adsorption on the iron oxyhydroxides goethite (α-FeOOH), akaganeite (β-FeOOH), and lepidocrocite (γ-FeOOH): A ^{31}P NMR Study, Energy Environ. Sci. 4 (2011) 4298–4305.

[5] R. Chitrakar, S. Tezuka, A. Sonoda, K. Sakane, K. Ooi, T. Hirotsu, Phosphate adsorption on synthetic goethite and akaganeite, J. Colloid Interface Sci. 298 (2006) 602–608.
[6] S. Yao, J. Li, Z. Shi, Phosphate ion removal from aqueous solution using an iron oxide-coated fly ash adsorbent, Adsorpt. Sci. Tech. 27 (2009) 603–614.
[7] Y.-S. Chen, W.-C. Chang, S.-H. Chuang, S.-M. Chiang, Comparison of kinetic models for predicting phosphate adsorption onto spent alum sludge in a continuous fixed-bed column, Desalin. Water Treat. 32 (2011) 138–144.
[8] N. Chen, C. Feng, Z. Zhang, R. Liu, Y. Gao, M. Li, N. Sugiura, Preparation and characterization of lanthanum(III) loaded granular ceramic for phosphorus adsorption from aqueous solution, J. Taiwan Institute Chem. Eng. 43 (2012) 783–789.
[9] R. Chitrakar, S. Tezuka, A. Sonoda, K. Sakane, K. Ooi, T. Hirotsu, Selective adsorption of phosphate from seawater and wastewater by amorphous zirconium hydroxide, J. Colloid Interface Sci. 297 (2006) 426–433.
[10] R. Chitrakar, S. Tezuka, A. Sonoda, K. Sakane, K. Ooi, T. Hirotsu, Adsorption of phosphate from seawater on calcined MgMn-layered double hydroxides, J. Colloid Interface Sci. 290 (2005) 45–51.
[11] L. Zeng, X. Li, J. Liu, Adsorptive removal of phosphate from aqueous solutions using iron oxide tailings, Water Res. 38 (2004) 1318–1326.
[12] T. Leiviskä, S. Gehör, E. Eijärvi, A. Sarpola, J. Tanskanen, Characteristics and potential applications of rough clay fractions from Puolanka, Finland, Cent. Eur. J. Eng. 2 (2012) 239–247.
[13] C.W. Bale, P. Chartrand, S.A. Degterov, G. Eriksson, K. Hack, R. Ben Mahfoud, J. Melancon, A.D. Pelton, S. Petersen, FactSage thermochemical software and databases, Calphad 26 (2002) 189–228.
[14] Y.-S. Ho, Isotherms for the sorption of lead onto peat: Comparison of linear and non-linear methods, Pol. J. Environ. Stud. 15 (2006) 81–86.
[15] A. Shvarzman, K. Kovler, I. Schamban, G. Grader, G. Shter, Influence of chemical and phase composition of mineral admixtures on their pozzolanic activity, Adv. Cem. Res. 13 (2001) 1–7.
[16] S. Shoval, M. Boudeulle, S. Yariv, I. Lapides, G. Panczer, Micro-Raman and FT-IR spectroscopy study of the thermal transformations of St. Claire dickite, Opt. Mater. 16 (2001) 319–327.
[17] F. Brunk, Silica bricks, in: G. Routschka (Ed.), Pocket Manual, Refractory Materials, Vulkan-Verlag, Essen, 1997.
[18] J.R. Odilon Kikouama, K.L. Konan, A. Katty, J.P. Bonnet, L. Baldé, N. Yagoubi, Physicochemical characterization of edible clays and release of trace elements, Appl. Clay Sci. 43 (2009) 135–141.
[19] M. Kosmulski, The pH-dependent surface charging and points of zero charge V. Update, J. Colloid Interface Sci. 353 (2011) 1–15.
[20] L.W. Zelazny, L. He, A.M. Vanwormhoudt, Charge analysis of soils and anion exchange, in: P.A. Maurice (Ed.), Environmental Surfaces and Interfaces from the Nanoscale to the Global Scale, John Wiley & Sons, Hoboken, NJ, 2009.
[21] S.C. Ayaz, O. Aktas, N. Findik, L. Akca, Phosphorus removal and effect of adsorbent type in a constructed wetland system, Desalin. Water Treat. 37 (2012) 152–159.
[22] O. Hamdaoui, E. Naffrechoux, Modeling of adsorption isotherms of phenol and chlorophenols onto granular activated carbon part I. Two-parameter models and equations allowing determination of thermodynamic parameters, J. Hazard. Mater. 147 (2007) 381–394.